Final submitted version of

Roncoroni, M. and Lane, S.N., 2019. A framework for using Unmanned Aerial Vehicles (UAVs) and SfM photogrammetry to detect salmonid redds. Ecological Informatics, 53, 1-18

https://www.sciencedirect.com/science/article/pii/S1574954119300512

A framework for using small Unmanned Aircraft Systems (sUASs) and SfM photogrammetry to detect salmonid redds

Matteo Roncoroni & Stuart N. Lane

Institute of Earth Surface Dynamics, University of Lausanne, Géopolis, Quartier Mouline, 1015 Lausanne, Switzerland

Correspondence to: M. Roncoroni matteo.roncoroni@unil.ch

Abstract

Salmonid populations are widely distributed globally and are of economic, cultural and ecological importance. Evidence suggests that they are in decline in many parts of the world and one of a number of hypotheses for their decline is the degradation of spawning habitat. Knowledge of spawning sites and their evolution through time is a means of estimating regional population dynamics and sizes. Traditionally, spawning sites have been identified visually. However, this may not allow a precise quantification of the real extent of salmonid reproduction and of its evolution through time (i.e. within the spawning season). This paper develops a framework for using small Unmanned Aircraft Systems (sUASs) and Structure from Motion (SfM) photogrammetry to detect salmonid redds, the nests that are the distinctive footprint of spawning, through analysis of inter-epoch Digital Elevation Models (i.e. DEMs of Difference). SfM-derived DEMs of Difference are an effective tool to investigate spawning because of the distinctive ellipsoidal erosion-deposition pattern of salmonid redds, which discriminates them from other stream-bed elevation changes. The method detects more redds (e.g. those covered by algae or biofilm) compared with classical visual observation, allowing for a better and more rigorous detection of spawning grounds. SfM photogrammetry also provides additional information relevant to understanding salmon spawning, including redd-density and probable female lengths, without disturbance of the spawning sites.

Key words: sUAS; Structure-from-Motion (SfM); Digital Elevation Model (DEM); DEM of Difference (DoD); Salmonid spawning; Redd

1. Introduction

Salmonid populations are widely distributed globally (Elliot, 1994; Crisp, 2000) and are of economic, ecological and cultural importance (Crisp, 2000), in particular the genera *Salmo* (e.g. brown trout or Atlantic salmon) and *Oncorhynchus* (e.g. rainbow trout or Pacific salmons). For example, the Pacific Northwest ecosystem relies on salmon migration for direct food provision (e.g. bears, eagles, etc.) and soil fertilization (Quinn, 2005), meaning that the hypothetical disappearance of salmonids might trigger serious negative effects. The preservation of salmonid populations is fundamental to maintain their ecological, economic and cultural roles in the various ecosystems they inhabit.

Salmonid populations are reported as being at risk for a range of reasons across the northern hemisphere, including Switzerland (Borsuk et al., 2006; Zimmerli et al., 2007), the British Isles (Hendry, 2003) and the Pacific Northwest (Bradford and Irvine, 2000; Simenstad and Cordell, 2000; Quinn, 2005; Bisson et al. 2009). These risks relate to a range of drivers, including climate change, over-fishing, water quality and habitat degradation (Crisp, 2000). One of many hypotheses for population decline (Kondolf et al., 2008) is the degradation of spawning grounds. However, there are fewer data on the presence and number of spawning sites and their changes through time even though such data are likely to contribute to understanding and managing regional population dynamics (Rieman and McIntyre, 1996; Gallagher and Gallagher, 2005; Murdoch et al., 2010; Howell and Sankovich, 2012).

The most common method for detecting and counting salmonid spawning sites remains walking along river banks during the spawning season and making visual observations of the nests, redds, made by salmonids (e.g. Crisp and Carling, 1989; Gallagher and Gallagher, 2005; Riedl and Peter, 2013). This approach has some weaknesses. First, it is influenced by the experience of researchers (Dunham et al., 2001; Muhlfeld et al., 2006; Howell and Sankovich, 2012) and their ability to detect the signatures of redd morphology and sedimentology in riverbeds. Second, redds may be masked soon after their construction by sediments, periphyton and algae making them difficult to observe (Rieman and McIntyre, 1996; Maxell, 1999; Dunham et al., 2001).

Third, significant time is required to do such survey and many hundreds of meters of river bank may need to be walked to identify spawning at a meaningful spatial scale, the river reach, and ultimately the river-basin. At the river scale, redds are rarely concentrated in just one specific location; i.e. some can be upstream, other downstream, and the longer the length of river covered, the more accurate the redd count is likely to be (Rieman and McIntyre, 1996). Then, measurements may be needed in the same river several times during the spawning season, which may last for many weeks, to avoid bias in redd counts (Dunham et al., 2001). While the potential duration of the spawning season is commonly known, it is impossible to know exactly when a fish will spawn in the river being investigated; and redds may be progressively harder to see with time after their construction (Rieman and McIntyre, 1996; Gallagher and Gallagher, 2005), making a single end of season survey less rereliable. For these reasons, methods that facilitate more rapid redd counting over large areas may be of interest to the salmonid ecology community.

Developments in remote sensing technologies (Lejot et al. 2007; Westoby et al., 2012; Micheletti et al., 2015a; Micheletti et al., 2015b) provide an opportunity to improve current redd identification and counting methods. Some attempts at salmon redd counting have been made using unmanned aircraft systems (Groves et al., 2016). In Groves et al. (2016) use of UASs allowed visual interpretation of images to replace visual identification by walkover (Groves et al., 2016). Here, we go one-step further by showing how it is possible to detect redds using digital elevation data acquired using small Unmanned Aircraft Systems (sUASs) and automated image processing methods.

Recent research in fluvial remote sensing (Tamminga et al., 2015; Woodget et al., 2015; Dietrich, 2016; Marteau et al., 2017) has shown that the morphology of shallow-water streams can be quantified using a combination of sUASs and Structure-from-Motion (SfM) photogrammetry, the latter used to extract three-dimensional morphological data (Digital Elevation Models or DEMs). By comparing DEMs through time (DEMs of difference), changes can be detected. As redds have a distinctive morphological signature, an ellipsoidal shape characterized by a depression upstream and an accumulation downstream (e.g. Crisp and Carling, 1989), DEMs of Difference (DoD) could be a means of quantifying the presence of redds.

The principal aim of this research is to develop a framework for the use of sUASs in detecting salmonid redds using photogrammetrically-based processing of acquired images. Redds need to be counted (Rieman and McIntrye, 1996), and this new framework should be able to do it in an easier and much more accurate way, as well as for larger spatial and temporal scales. A second and subsidiary aim is to show that such information can be used to enhance our knowledge of salmonid spawning processes. This information includes knowledge of redd densities, redd locations on the riverbed, possible female lengths, timing of spawning and egg burial depths, elements crucial for fish biology (Crisp and Carling, 1989). A key advantage here is that it may be possible to acquire data without entering the water and so avoiding redd disturbance (e.g. movement of fines, etc.). The focus of the work are the redds of *Salmo trutta*, or brown trout, which is naturally present in the southern Switzerland. However, the framework is extendible to other salmonid species given that all build nests with a particular morphological signature.

The paper begins by detailing the information that our framework should be capable of providing in relation to salmonid redds. Then we present an overarching framework for this kind of approach, making reference to established research on how to produce precise, high resolution 3D data on streambed morphology and its change through time. We detail the methodology that we used to test this framework for brown trout redds. The results are presented for the case-study and discussed in the final sections of the paper.

2. Spawning of brown trout and the structure of salmonid redds

In order to understand the methodology proposed in this research, it is necessary to review briefly our current understanding of brown trout spawning and the structure of salmonid redds. The former identifies when sampling is needed and the latter provides critical information on the target precision and resolution of acquired data, and hence the required design of the image surveys. Such analyses would need to be undertaken for the target salmonid population if not brown trout.

2.1 Timing, spawning and construction of the redd

Spawning of brown trout takes place each year, generally from autumn to late winter in the northern hemisphere (Armstrong et al., 2003). Swiss populations of brown trout tend to spawn from October to January (Riedl and Peter, 2013). Spawning time depends on altitude (Riedl and Peter, 2013) and mean water temperature (Heggberget et al., 1988; Webb and McLay, 1996; Klemetsen et al., 2003). Consequently trout spawning occurs earlier at higher altitudes (Riedl and Peter, 2013). Reproduction involves two main stages: (1) search for the ideal site and erosion of the streambed by a female trout; and (2) deposition, fertilization and burial of eggs.

In the first stage, the female trout searches for a site where conditions for spawning are apparently present (Crisp and Carling, 1989; Crisp, 2000), and these conditions are a function of water velocity, water depth and grain-size (Armstrong et al., 2003). Additional parameters shown to be important include the ease of disturbance of the substratum (Kondolf, 2000) and the presence of a local down- or up-welling of flow (Burner, 1951; Healey, 1991). In order to check the conditions, the female erodes the streambed with tail fin motions, creating a depression called a pit, displacing the grains just downstream (Crisp and Carling, 1989; Crisp, 2000). In this way, the female trout can check local conditions and evaluate their suitability (Crisp, 2000). While the female erodes the streambed, one (normally the dominant) or more males stay in the proximity of the female waiting to fertilize the eggs (Crisp and Carling, 1989; Elliot, 1994; Crisp, 2000). If the conditions remain suitable after the initial erosion, the female increases the erosion (Crisp and Carling, 1989) and the second stage begins.

At the beginning of the second stage, the female continues to erode the streambed more and more frequently while the dominant male drives away the beta males (Crisp and Carling, 1989; Crisp, 2000). At that point, the female lays the eggs while the male fertilizes them (Elliot, 1994; Crisp, 2000). The female then buries them with sediments created by erosion of the surrounding streambed (Crisp and Carling, 1989). This process may be repeated several times in the same spawning process, creating more pockets of eggs in the same redd (Crisp and Carling, 1989; Crisp, 2000). During the final burial stage, the female continues to cut the streambed in order to complete burial but with a low frequency, while the males move away (Crisp and Carling, 1989). The result is a salmonid redd created on the streambed.

2.2 Redd structure

A salmonid redd is recognizable (Crisp and Carling, 1989) by its ellipsoidal shape, with a depression upstream, called a pit, and an accumulation downstream, called a tail (Figure 1). The tail volume is related to the volume of the pit because it results entirely from the displacement of the grains from the pit. The redd size is related to the size of the female trout (Crisp and Carling, 1989) and the dimension increases with the increment of female length: the redd size is approximately 3.5 times longer than the female length (Crisp, 2000). Following Crisp and Carling (1989) it is possible to estimate redd length from female length (and vice versa) in a more rigorous approach using different parameters (see Section 4.6). In the same way, it is possible to estimate other horizontal dimensions (e.g. pit and tail width). In the literature there is no evidence regarding the estimation of the vertical dimensions, such as pit depth and tail height. However, Grost et al. (1991) found that pit depths normally range between 0.07 to 0.34 m while tail heights vary between 0.03 and 0.25 m.

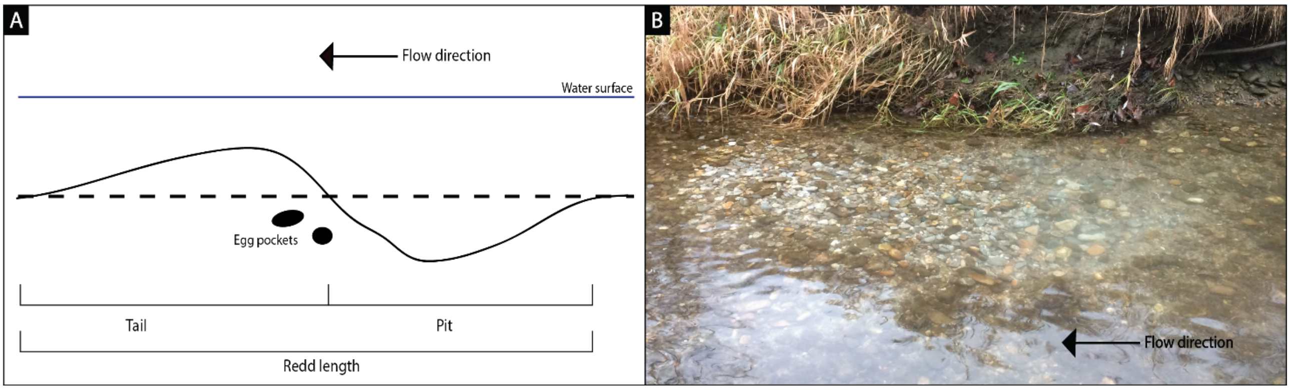

Figure 1 : A) Schematic structure of a redd (modified from Crisp and Carling, 1989); B) Brown trout redd on Ticino River (Switzerland)

3. Development and justification of a framework for redd detection

3.1 Image acquisition platforms

The imagery needed for survey needs to be near nadir because of refraction at the water surface and available at the scale of 100s of meters to kilometers. This requires an airborne image acquisition platform. Helicopters are a solution (e.g. Carbonneau et al., 2004, 2005; Bergeron and Carbonneau, 2012; Dietrich, 2016), but are expensive, prohibiting repeat data acquisition. The emergence of small UASs in science provides an alternative, low-cost and flexible method to acquire images (Lejot et al., 2007; Carbonneau et al., 2012; Groves et al., 2016).

3.2 Extraction of elevation data

SfM photogrammetry has emerged in river research (e.g. Tamminga et al., 2015; Woodget et al., 2015), as an alternative to classical digital photogrammetry (e.g. Lane et al., 2000) as it is rapid, automated, low-cost and easy to use by non-experts (Fonstad et al., 2013; Woodget et al., 2015). If correctly applied it can produce high quality DEMs (e.g. Westoby et al., 2012; Fonstad et al., 2013), of a similar quality to those produced by airborne LiDAR (Fonstad et al., 2013).

As with classical digital photogrammetry, SfM produces 3D data from overlapping images (Westoby et al., 2012; Fonstad et al., 2013). However, unlike traditional aerial photogrammetry, where images overlap in parallel strips captured from parallel flights (Fonstad et al., 2013), SfM photogrammetry can use overlapping images captured from any given point of view (Westoby et al., 2012; Fonstad et al., 2013). As with terrestrial photogrammetry (Lane et al., 1994), oblique imagery can be used, but such imagery can be problematic for river research as it increases the probability of reflection at the water surface due to refraction. SfM facilitates processing by using machine vision methods which can produce good results even with very low-grade quality sensors such as smartphones (e.g. Micheletti et al., 2015b).

As with classical photogrammetry SfM uses the collinearity equations to describe the three-dimensional relationship between the sensor position and orientation and the ground surface (Fonstad et al., 2013; Woodget et al., 2015). In traditional photogrammetry the collinearity equations are solved in what is called a bundle adjustment after the introduction of Ground Control Points (GCPs). In SfM photogrammetry these equations can be solved without GCPs and the derived data scaled from an arbitrary to an actual coordinate system later (Fonstad et al., 2013).

Introducing GCPs after a preliminary bundle adjustment, to aide GCP measurement on imagery, and then re-running the bundle adjustment may improve solution of the collinearity equations (James et al., 2017a). After solution, machine vision methods are used to identify conjugate points (the same point visible on at least two images) and through application of the collinearity equations determines coordinates of those points. Typically, the point clouds that result have an average spacing that is 3 to 5 times the image pixel resolution.

3.3 Theoretical precision and flying height

The design of image acquisition has to be based upon the target measurement precision for the elevation data needed to detect redds. The size of redds is likely to vary as a function of female lengths (Bjorn and Reiser, 1991), as well as of species: for example, brown trout (*Salmo trutta*) redds are smaller than those of Chinook salmons (*Oncorhynchus tshawytscha*) (see Reiser and Wesche, 1977; Neilson and Banford, 1983). This size should be used to inform survey design. In principle, to reduce data acquisition and processing times, imagery should be flown with as coarse a resolution as possible given the surface changes that are to be detected. Under the assumption that errors in Digital Elevation Model (DEM) are random, Gaussian and independent, a change in elevation between two dates has an uncertainty (U_{crit}) defined by:

$$U_{crit} = \pm t\sqrt{(\sigma_i)^2+(\sigma_j)^2} \qquad [1]$$

where t is set for a given confidence interval, here taken as 95% (so t = 1.96) and σ_i and σ_j are the precisions of elevation of the two analysed DEMs (e.g. Lane et al., 2003). In classical photogrammetry, it is well established that the theoretical precision of DEM elevations is approximately the same as the image resolution *R* (e.g. Lane et al., 2010). Research suggests that in SfM photogrammetry, this may be downgraded to be about 10% higher but also spatially variable reflecting the difficulties that SfM has in recovering camera geometry precisely (James et al., 2017b). Here, we use R as the elevation precision noting that achieving this value of *R* requires careful attention to be given to image acquisition geometry and that *H* in [5] below should be set as a maximum given that precision may be degraded in when using sUASs with SfM photogrammetry.

Under the assumption that the images are both acquired with the same study design:

$$U_{crit} = \pm 1.96\sqrt{2R^2} \qquad [2]$$

Thus, the image resolution required to detect change is:

$$R = \left[0.5\left(\frac{U_{crit}}{1.96}\right)^2\right]^{0.5} \qquad [3]$$

R can be defined approximately through:

$$\frac{p}{f} = \frac{R}{H} \qquad [4]$$

where *p* is the sensor pixel resolution, *f* is the sensor focal length and *H* is the sensor flying height. Thus, we can determine the *H* needed in the first flight path to obtain a given U_{crit} as:

$$H < \frac{f}{p}\left[0.5\left(\frac{U_{crit}}{1.96}\right)^2\right]^{0.5} \qquad [5]$$

Use of [5] should be accompanied with visual inspection of acquired imagery to make sure that with this value of *H* there is the texture in the acquired imagery needed for the machine vision methods to work. Note that [5] implies that the derived precision is not simply a function of the flying height, but is also impacted by *f* and *p*. As technology progresses (and *p* in particular falls), use of [5] should remain robust unlike use of simple multiples of flying height alone.

3.4 Image acquisition geometry

Whilst [5] may determine the minimum flying height needed for change detection, this does not deal with the potential problem of systematic error in DEM surfaces which can arrive due to uncertainties in sensor position and orientation (e.g. Lane et al., 2004) as well as poorly reconstructed sensor geometry. The latter has been found to be a particular issue with small UASs as these tend to use low grade sensors with high levels of distortion and lead to artefacts in derived DEMs such as doming (Fonstad et al., 2013; James and Robson, 2014; Carbonneau and Dietrich, 2017). As shown by Wackrow and Chandler (2011), James and Robson (2014) and Carbonneau and Dietrich (2017), such errors may be reduced through careful design of flight paths, to include convergent images, multiple flight altitudes and a high degree of image overlap. The basic principle here is to reproduce the kind of geometries long-used for calibration of non-metric cameras in photogrammetry (e.g. Robson, 1992). An example is shown in Figure 2, which combines at least two flying heights with some off-nadir imagery and two differently oriented flight paths (as not all geometrical distortions in the sensor are symmetrical) and which lead to convergent views. A minimum overlap of 70% is required for photogrammetric analysis but increasing the level of overlap to as high as 90% may improve calibration. Finally, the sUAS flight velocity should not be so high that it introduces image blurring, which results from forward speeds that are too high for a given exposure time.

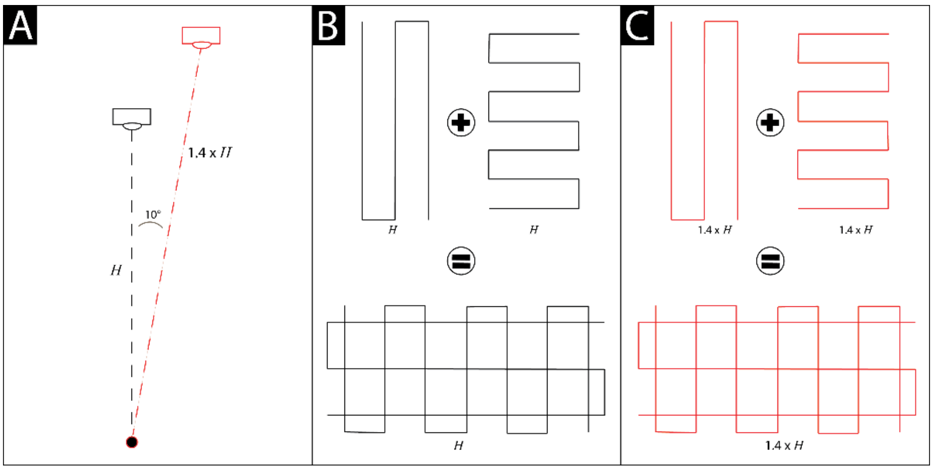

Figure 2: Flight strategy following Wackrow and Chandler (2011), James and Robson (2014) and Carbonneau and Dietrich (2017). A) Frontal view of two single acquisitions points where H = flight altitude of the 1st flight and 1.4 x H = flight altitude of the 2nd flight; B) Upper view of the flight path grid at H; C) Upper view of the flight path grid at 1.4 x H.

3.5 Ground control points

Early applications of SfM photogrammetry claimed that it may eliminate the need for Ground Control Points (GCPs) to be installed prior to image acquisition and that only a small number would then be needed for addition *a posteriori* if absolute orientation, position and scale were required (Fonstad et al., 2013). However, it has been shown that carefully located GCPs can improve solution of the collinearity equations so reducing systematic error (James and Robson, 2014) and improve morphological change detection (e.g. Woodget et al., 2015). For orientation, position and scale, at least 3 GCPs are needed (e.g. Woodget et al., 2015) but more may help to avoid erroneous data transformations (Westoby et al., 2012) and ultimately to reduce systematic error (James et al., 2017a) (Figure 3).

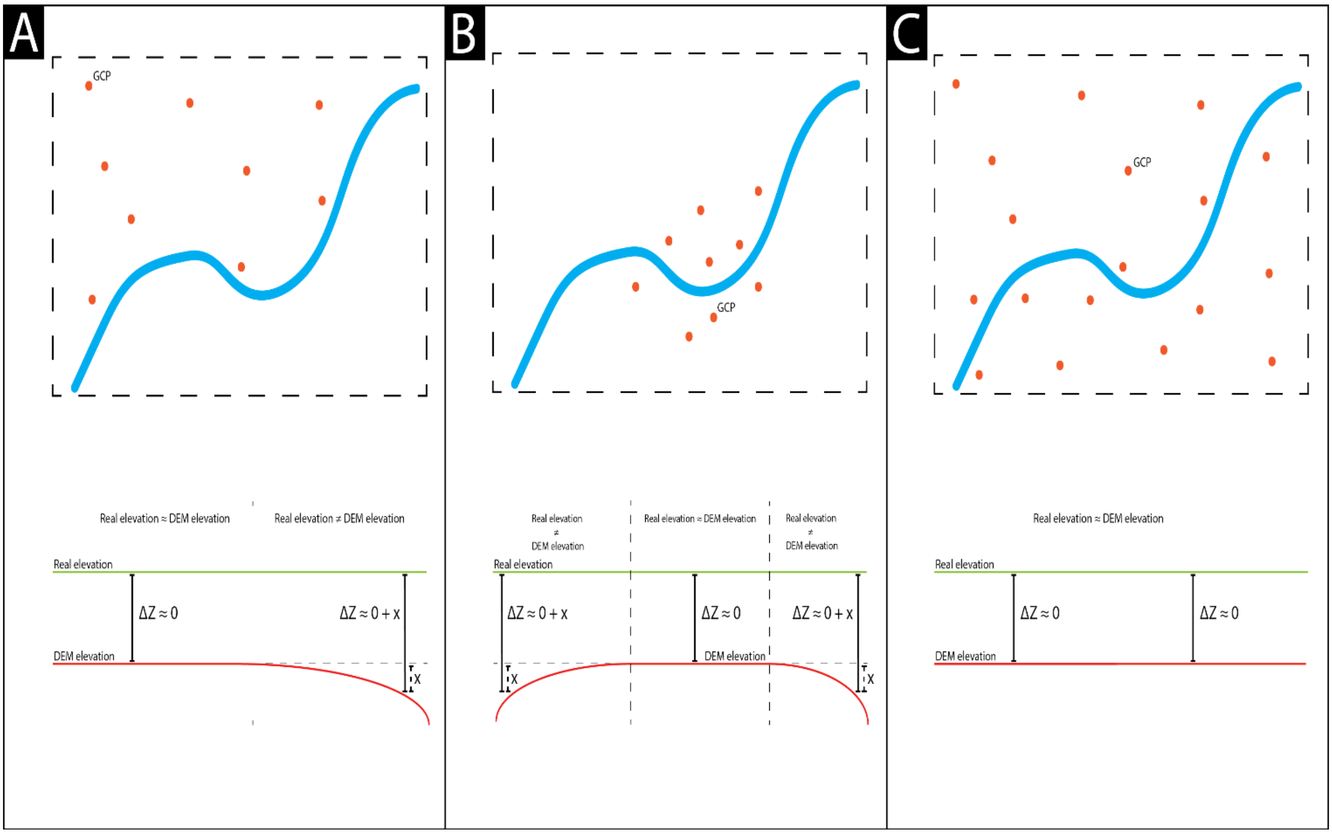

Figure 3: Systematic error may not be reduced with poorly-placed GCPs. In 3A, GCPs are located only on one side of the river creating a non-regular tilt effect of ΔZ=0+x (where x is the difference between the real elevation and DEM elevation for the same spatial point) on the other side. In 3B, GCPs are located in the centre of the study area creating a non-regular tilt effect of ΔZ=0+x on the both sides of the area (similar to

doming effect). In 3C, GCPs are scattered across the study area better constraining the results and reducing the level of systematic error.

3.6 Post-processing: bathymetric correction

A crucial stage in automated redd detection using DEMs is the correction for the effects of refraction at the air-water interface. This is a well-established problem in river studies (e.g. Fryer, 1983; Fryer and Kniest, 1985; Westaway et al., 2000, 2001; Butler et al., 2001; Dietrich, 2017). The magnitude of refraction changes as a function of flow depth, and hence discharge, and so if data are collected on two different dates, with different discharges, the effect has to be removed from both datasets for true changes to be detected. Tamminga et al. (2015) and Woodget et al. (2015) used a simple procedure to correct submerged areas of DEMs based on SfM photogrammetry with near-nadir imagery. The principle follows Westaway et al. (2000): an uncorrected DEM is subtracted from the water surface elevations, the result is multiplied by the refractive index of clear water and then the new result is subtracted again from prior water surface elevations in order to produce a corrected DEM. Following the more complex approach of Westaway et al. (2001), Dietrich (2017) developed this approach for SfM photogrammetry (Dietrich, 2017). Dietrich's approach is based on the correction of each wet-point in the point cloud by solving the refraction equations for each camera that sees the wet-point itself and by then iterating the equations to convergence. This per-camera and iterative approach is needed because each wet-point may be seen from more than two images, each with different flight altitudes and camera angles.

3.7 Redd detection: from visual detection to morphological change detection

Switching from visual to morphological analysis needs two issues to be addressed. The first requires removal of any residual systematic error in the derived DEMs that has not been minimized through the chosen image geometry. Such error may be manifest in validation data, or when two DEMs are compared and zones of no known change show apparent erosion or deposition. As such error is systematic, it can normally be modeled (e.g. using a two dimensional, non-linear fit to data that should show no change) and then removed. The second is addressed after removal of systematic error and involves quantifying the probable limits of detection (Brasington et al., 2000; Fuller et al., 2003; Lane et al., 2003; Wheaton et al., 2010; Milan et al., 2011) in the data. The simplest approach uses [1] but replaces the theoretical precisions with some measure of the actual elevation precisions achieved, under the assumption that the errors are Gaussian, random and pairwise independent (Lane et al., 2003; Fisher and Tate, 2006). Such thresholding may be harsh to datasets, especially where changes are small in magnitude but spatially extensive and coherent (Wheaton et al., 2010). To assess the quality of morphological detection, orthoimages may also be used. Redds visible in the orthoimages (i.e. those that are not masked) should also be reflected in the DoD. If this is not the case, the DoD quality should be questioned, and it may be concluded that the vertical precision of one or both of the derived DEMs was not sufficient.

4. Materials and methods

4.1 Case study

We applied and tested the above framework for a Swiss stream, the Breggia, that flows through the southern part of Canton Ticino (Figure 4). The Swiss part of the Breggia has a catchment area of c. 81 km^2. The study site (Figure 4) is located northeast of Chiasso, in the lower part of Breggia, *c.* 3 km from Lake Como. Here, the Breggia flows through an urban area and its channel has been straightened, with concrete banks. We chose this small reach (~70 m) mostly for three reasons: i) it is known to be a potentially important reach of the Breggia for spawning; ii) the small size compared with other upstream reaches allows us to focus upon testing the processing and post-processing phases, even though the method may be extendable to larger spatial scales compared with those used here; and iii) reach depths did not exceed *c.* 0.45 m (except for the deep pool upstream of the reach $\overline{x}_{depth}$ = 0.48 m; $\tilde{x}_{depth}$ = 0.41 m; σ_{depth} = $\pm$0.2 m) leading to a more effective bathymetric correction. The ease of applying the method over large scales may be limited by regulations regarding drone use, such as those that require lone of sight to be maintained.

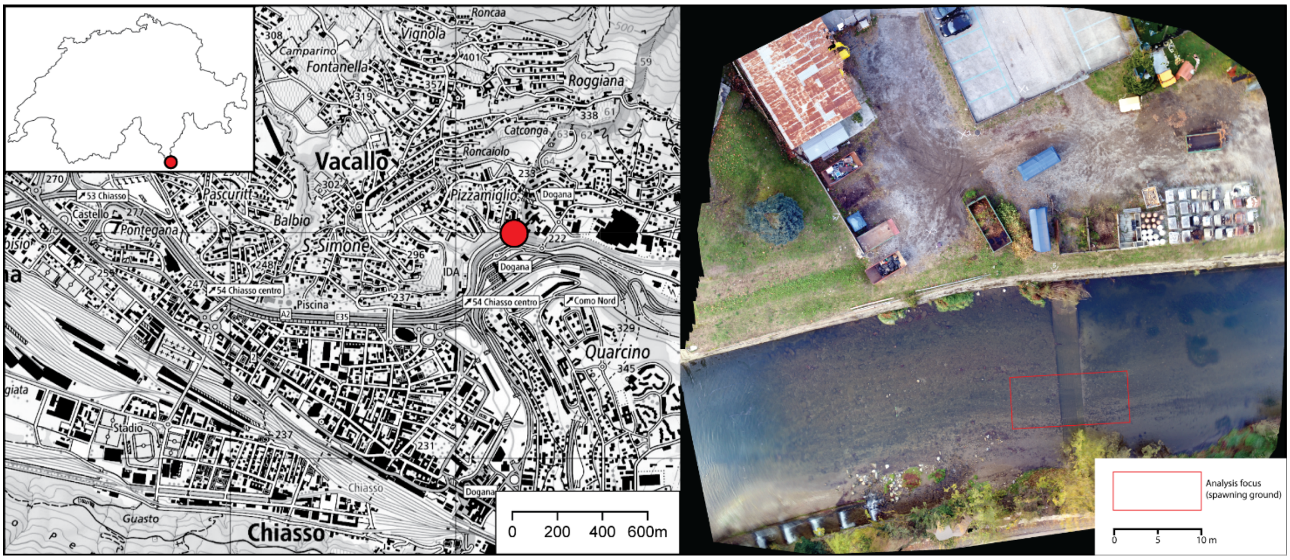

Figure 4: On the left, localization map of the studied zone (©swisstopo). On the right, orthomoisaic of the zone with boundaries of the focused area of interest. All of our further analysis (e.g. DoD) will be performed only on the focused area.

We surveyed the reach 8 times during the spawning season between Oct. 7th and Dec. 30th 2017 (Oct. 7th, Oct. 20th, Oct. 28th, Nov. 11th, Nov. 19th, Dec. 2nd, Dec. 10th, Dec.

23rd and Dec. 30th), with a mean time interval between survey dates of 9.5 days. Here we present data for three dates (Nov. 19th, Dec. 2nd and Dec. 10th): we did not identify redds before Nov. 19th and, in the same way, we did not identify redds after Dec. 10th, although this was partly due to important sediment accumulation in the reach between Dec. 10th and 23rd caused by in-stream works in the upper Breggia.

4.2 Image and GCP acquisition

We acquired images with a DJI Phantom 3Pro quadcopter. This drone is low cost, easy to use, lightweight, easy to transport and it has a built in GPS. Software is available to aid flight planning which is necessary to make sure that imagery has the required resolution, coverage and geometry.

We planned flight paths with Pix4Dcapture (Pix4D, 2017a). We set U_{crit} of ± 0.024 m on the basis of expected bed level changes due to redd construction by brown trout, that generally are bigger than 0.03 m (Grost et al., 1991). This corresponds to a flight altitude of ~20 m with a Phantom 3Pro. We flew two flights paths at this altitude and two additional flight paths at 30 m. To allow for convergent images, we oriented all four flight paths orthogonally, and set the second of the two flight paths to have an off nadir view (see Figure 3). We emphasise that an off nadir view does not necessarily imply convergent imagery. With the drone control software we were using, the drone turns through 180° at the end of each flight line and this allowed us to acquire imagery with different view angles.

We painted GCPs on stable zones using a biodegradable white paint, with a small red dot as a permanent marker. The white cross disappeared between surveys but the red dot remained so we could repaint the GCPs in subsequent visits. We painted 5 GCPs and measured using a Trimble R10 dGPS. We installed a permanent base in case we needed to remeasure GCPs. No reoccupation was needed as the 5 GCPs were all detectable on later visits. We then processed the data to the Swiss CH1903+ coordinate system. Note that with the use of only 5 GCPs our survey design may not remove doming; rather it is improving the precision with which the point derived clouds are registered to the ground. For this reason, below, we discuss the additional systematic error removal that was needed. Collecting more ground control points was a challenge because we did not have permission to survey the Italian side of the river. Similarly, we did not acquire in-water validation points to assess submerged DEM quality because this would have required crossing an international frontier to obtain data, which would have also needed additional permissions. As we note below, such data may be valuable for validating DEMs, but are not necessarily suitable for validating DEMs of difference.

4.3 SfM photogrammetric processing

We used Pix4Dmapper (Pix4D, 2017b) for the SfM photogrammetry. In an initial step, conjugate features were identified by the software across multiple images and to provide a provisional calibration of internal (i.e. focal length, principal point offsets, lens distortion) and external (i.e. image position and orientation) camera parameters. We then generated an initial sparse point cloud was generated and an orthoimage, which we used to help to insert GCPs before we re-ran the calibration. In the second step, the sparse point cloud was densified by the software to obtain a dense point cloud. In the third step we interpolated the DEM to ~0.043m resolution and produced an orthoimage free of perspective distortions (~0.008m resolution). An important by-product of all steps, but notably Step 1, is a quality report, which we used to assess the fidelity of the photogrammetric solution.

4.4 Bathymetric correction

To deal with water refraction, we applied Dietrich's (2017) bathymetric correction method. First, we modeled the water surface from water edge data using kriging in a GIS framework. Second, we used the associated water surface to identify DEM elevations that were inundated. These were exported. Data on the relative positions and calibration of each image were exported from Pix4D. Each DEM point was then corrected. The only parameter that this analysis requires is the refractive index of water, which is here taken as 1.337 (Harvey et al., 1998). We then recombined them with the elevations from non-inundated zones in the GIS to produce a corrected DEM.

4.5 DEMs of Difference

We calculated DEMs of difference (DoDs). Initial visualization of the results suggested that there was a residual systematic error, notably revealed by changes where there should have been none (e.g. in large boulders that would not have moved between the dates of acquisition). This systematic error was caused by the absence of GCPs on the right bank (Italy), and the consequent poor transformation to the co-ordinate system being used. Hence, the DEMs describing the channel were shifted compared with the absolute coordinate system (Figure 3A). Additionally, the datum shift was different between survey dates because the acquisition conditions (e.g. light) were different during the surveys. Given the impossibility of registering all of the DEMs to an absolute reference, we decided to register them to the channel portion of a reference DEM which we took as the first DEM surveyed, before spawning began. Our changes are therefore with reference to this DEM. We used the freeware CloudCompare, to co-register the datasets to our reference DEM using an iterative closest point (ICP) algorithm (see Besl and McKay, 1992). The principle of the ICP is to identify shapes in one dataset and to register them onto those in the reference dataset by distance minimization using a least squares method (Besl and McKay, 1992). As datum shift could lead to erroneous bathymetric correction, we applied the correction after the bathymetric correction.

In order to calculate the actual DEM quality and hence the level of detection, we identified zones of no-known change (Figure 5) between the reference DEM and the analyzed DEMs. These zones of no-known change were submerged boulders that did not move during the surveys. Ideally, independently-acquired validation points might be used to do this. They could not be acquired in this case. Further, as it is the detected changes which we would want to validate, we would need to detect change at the same points by reoccupying them. Given the scales of surface variability (a function of grain size) and dGPS errors, such a dataset is likely to contain error and for this reason assuming that our method should produce no change in zones of no change is preferable. We compared the elevations and we calculated the standard deviations of error needed for [1]. Hence, we used elevations extracted from the reference DEM as they were independent variables to solve [1]. We explored the effects of both a 95% level of detection (i.e. 1.96 in [1]) but also a 68% level of detection. To produce DoDs we used our reference DEM (Nov. 11th), which was the closest in time to the first spawning event.

Figure 5: No-known change points (n=84). The points have been chosen by comparing orthoimages and DEMs. Points could also be collected on the concrete bar, which is immobile. However, water surface roughness created poor 3D reconstruction in this region so reducing the reliability of points in this zone.

4.6 Data on redd characteristics

We estimated female lengths and egg burial depths using data derived from both the DoDs and orthomosaics. We measured the tail of each redd and we used in an empirical relation to estimate female length and egg burial depth:

$$\ln T = b \ln L + \ln a \quad [6]$$

where L, the length of the female fish (cm), is defined by:

$$L = e^{\left(\frac{\ln a - \ln T}{-b}\right)} \quad [7]$$

T is the redd tail length (cm), and ln a and b are constants (for the genus *Salmo*: b = 1.2 ±0.2 and ln a = 0.45 ±0.38) (Crisp and Carling, 1989). From [7] we estimated the basal main egg pocket burial depth following Ottaway et al. (1981):

$$B_{depth} = c + d \ln L \quad [8]$$

where B_{depth} is the basal main egg pocket burial depth, c and d are constants (c = -37.7 ±12.1 and d =14 ±3.3). We note that the semi-logarithmic relationship of Ottaway et al. (1981) was performed on the fork length of the female trout and not on the total length as in Crisp and Carling (1989) in [7]. However, we assume (mainly from photographs) that thr differences between the fork length and the total length of brown trout are negligible (in the adult and mature life-stages). The use of Ottaway et al.'s (1981) semi-logarithmic relationship instead of Crisp and Carling's (1989) linear regression to estimate egg burial depth is pertinent because we can derive the main basal depth and not the mean depth. In this sense, we are more interested in the estimation of the basal depth to understand egg loss from washout or overcutting by later spawning trout, if we know the approximate lower location of the main egg pocket. However, as noted by Crisp and Carling (1989), predictions of egg burial depths derived by both equations are normally similar. That said, burial depth estimation remains uncertain (Crisp and Carling, 1989; DeVries, 1997).

Measurements of redd tails were easier on the DoD due to a clear distinction between the erosion and deposition zones. However, an estimation of redd tail sizes was also possible from orthoimagery, even if this was more difficult and less precise than that done on DoD. Even if tail lengths were similar between the two measurement ways, we opted for the more rigorous DoD approach. We used as a starting point the first evidence of deposition (near the pit) and as end point the last depositional evidence, following the general angle of the redd itself.

We also noted that redds were constructed one on top of another and so it was also possible to look at the extent to which redd construction was leading to the washout of the eggs of previously constructed redds.

A summary of the key stages used here to detect redds and extract useful information is provided by Figure 6.

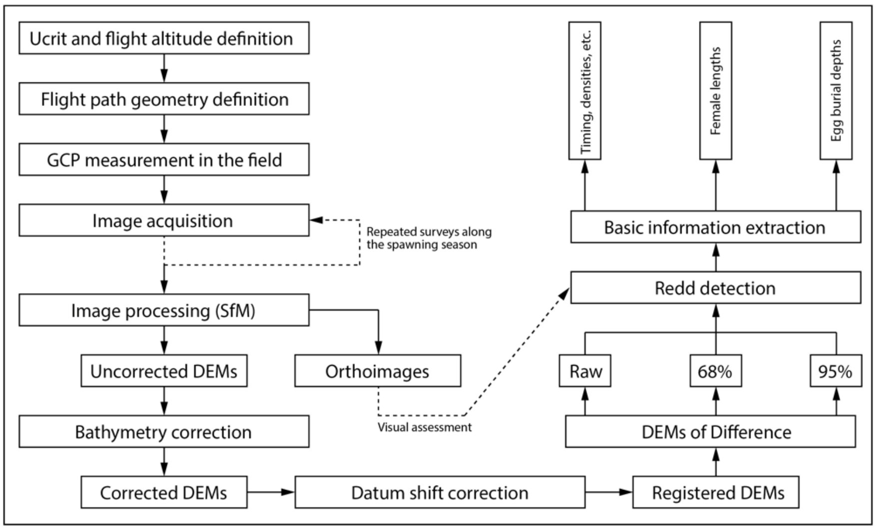

Figure 6: Summary of the methodological workflow and methods

5. Results

5.1 Illustration of data post-processing steps

Without prior correction of the datum shift and for underwater topography (Figure 7) the DoD is of no use for change detection: the DoD suggests that erosion is dominant in the all three situations which is not the case; although there appears to have been some more localised change that might suggest that spawning has occurred (e.g. in the bottom left of Figure 7A). Here, the datum shift is strongly negative, which means that the Z-coordinates of our analysed DEMs are located at a lower spatial position than the reference (Nov. 11th).

Figure 7: Raw DoD derived from original DEMs, therefore without bathymetry and datum shift corrections. Sub-figure A shows the situation between Nov. 11th and Nov. 19th, sub-figure B between Nov. 11th and Dec. 2nd and sub-figure C between Nov. 11th and Dec. 10th.

The DEMs of difference after datum shift correction (Figure 8) show that erosion is no longer dominant, and erosion and accumulation patterns are more balanced even if the latter is more present than the former (Figure 8A and C).

Figure 8: Raw DoD derived from DEMs with a first datum shift mitigation. Sub-figure A shows the situation between Nov. 11th and Nov. 19th, sub-figure B between Nov. 11th and Dec. 2nd and sub-figure C between Nov. 11th and Dec. 10th.

With correction of both datum shift and bathymetry (Figure 9) erosion and accumulation patterns become coherent. Comparison with the orthoimages shows that visually identifiable zones of possible spawning (Figure 10) correspond to vertical changes in the DoDs (Figure 9).

Figure 9: Raw DoD derived from bathymetry and tilt corrections DEMs. Sub-figure A shows the situation between Nov. 11th and Nov. 19th, sub-figure B between Nov. 11th and Dec. 2nd and sub-figure C between Nov. 11th and Dec. 10th.

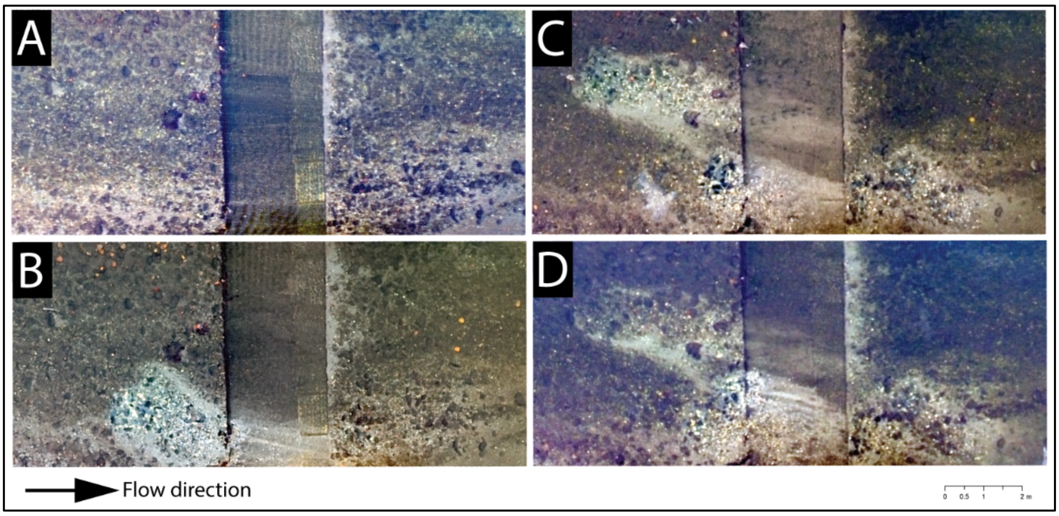

Figure 10: Orthomosaics of the spawning site. A) Nov. 11th; B) Nov. 19th; C) Dec. 2nd; D) Dec. 10th.

To assess the quality of the DoD results, Table 1 shows the mean and standard deviation of errors for zones of no-known change for the case of no treatment, datum shift only and datum shift combined with bathymetric correction. The distributions of error are shown in Figure 11.

Table 1: Mean errors and standard deviation of errors for the original DEMs calculated from the differences in elevations of fixed points (n=84) in zones of no change between the reference DEM (Nov. 11th) and the analysed DEMs.

No correction	Nov. 11th - Nov. 19th	Nov. 11th - Dec. 2nd	Nov. 11th - Dec. 10th
Mean (m)	-0.070	-0.128	-0.124
Standard Deviation (m)	±0.009	±0.016	±0.013
Datum shift correction			
Mean (m)	0.016	-0.007	0.015
Standard Deviation (m)	±0.007	±0.018	±0.014
Datum shift and bathymetric correction			
Mean (m)	-0.001	-0.003	-0.006
Standard Deviation (m)	±0.010	±0.015	±0.013

Table 1 shows that the mean errors decrease with each post-processing phase. As expected, the standard deviations of error (i.e. the variability about the means) do not change much, as both datum shift and bathymetric corrections remove systematic error rather than improve survey precision. The distributions confirm (Figure 11A) that before any kind of correction, errors are primarily negative. Datum shift correction does not eliminate systematic error fully and deviations still persist (Figure 11B). Finally, after both corrections, errors are well distributed around the origin (Figure 11C). Nov. 11th - Dec.2nd and Nov. 11th - Dec. 10th show small remaining negative deviation, but this is now very small and < 0.01 m.

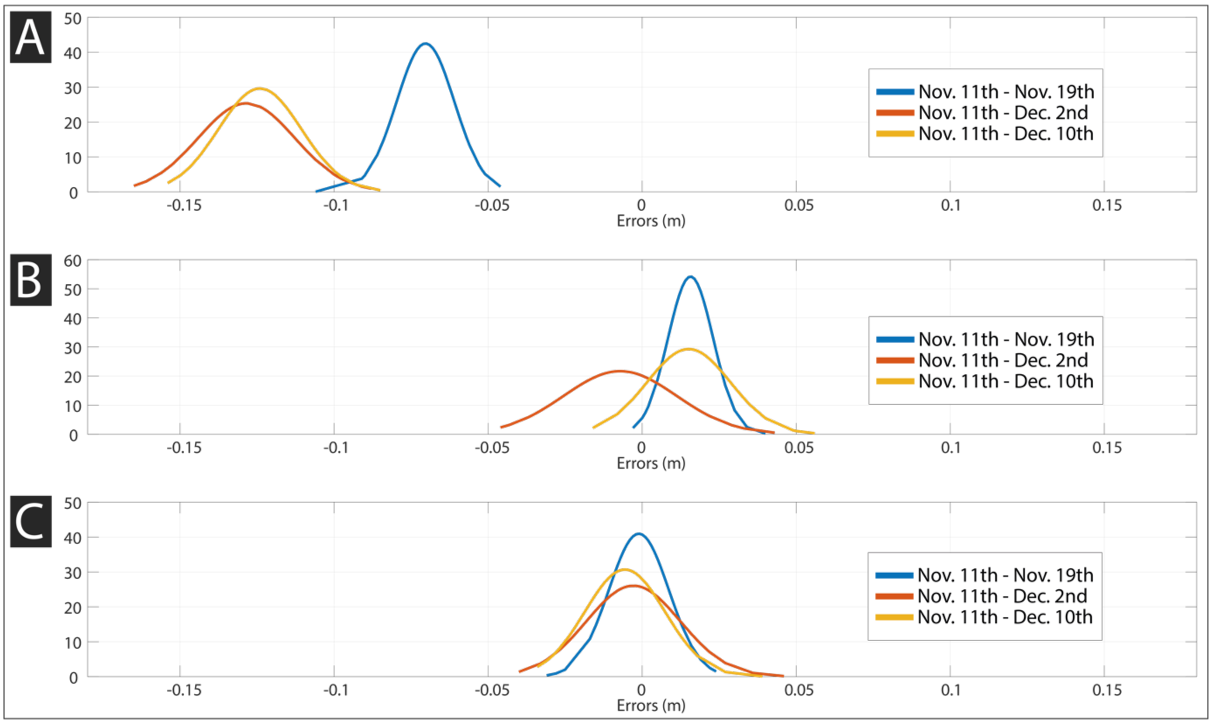

Figure 11: A) Error distributions for the original DEMs; B) For datum shift corrected DEMs only; C) For bathymetry ant datum shift corrected DEMs. All errors are calculated for zones of no change.

5.2 Redd detection

Figure 12 shows how redds disappear and new redds appear within the spawning season: the redd of Nov. 19th (Figure 12B) disappeared completely after 13 days (Dec. 2nd); the same happened to the redds that had then formed by Dec. 2nd (Figure 12C) compared with Dec. 10th; and on Dec. 23rd (Figure 12E) no redds were still visible at the site.

Apart from Dec. 23rd where deposition occurred, visual disappearance of redds in the reach were attributable to periphyton and algal growth. This makes sense considering that disturbances were not recorded before Dec. 23rd, and periphyton and algae were could develop on the streambed. The lower Breggia river has relatively high rates of primary production because upstream there is wastewater treatment plant which does discharge some nutrient-containing water.

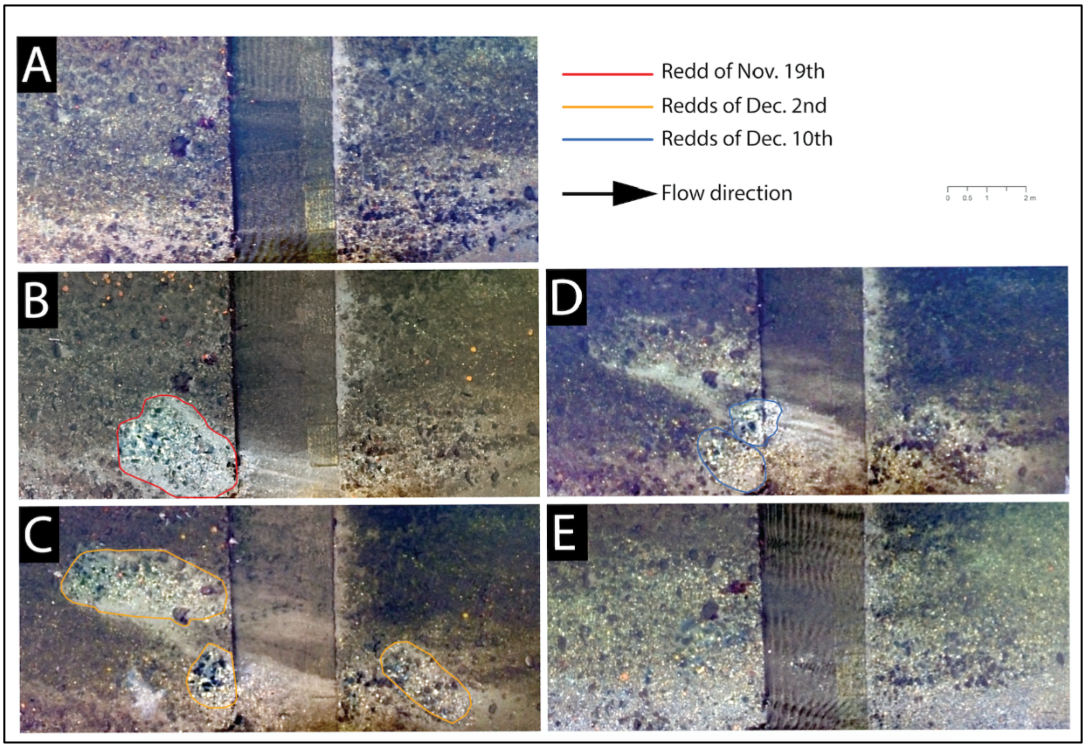

Figure 12: Evolution of the spawning site on the Breggia river throughout the 2018 season. A) Nov. 11th; B) Nov. 19th; C) Dec. 2nd; D) Dec. 10th; E) Dec. 23rd.

Figure 9 shows that it is possible to detect redd-related morphological changes. Some of them are confirmed by visual analysis of Figure 12. However, comparing Figures 9 and 12, it seems that more redds are present in the morphological analysis than in the visual one. Once a 68% level of detection threshold was applied (Figure 13), the redds become clearer and this 10 m reach of stream had a total of 9 redds that formed during the study period. These redds are much less clear when a 95% level of detection is applied (Figure 14) with only 8 of the 9 redds apparent in Figure 13 (see Table 2) and their morphology much less clear.

Table 2: Resumed results for the four different analyses performed on the Breggia spawning site.

Survey date	Nov. 19th	Dec. 2nd	Dec. 10th
Number of redds in the orthomosaics	1	3	2
Number of redds in the raw DoD	1	6	2
Number of redds in the 68% CL DoD	1	6	2
Number of redds in the 95% CL DoD	1	5	2

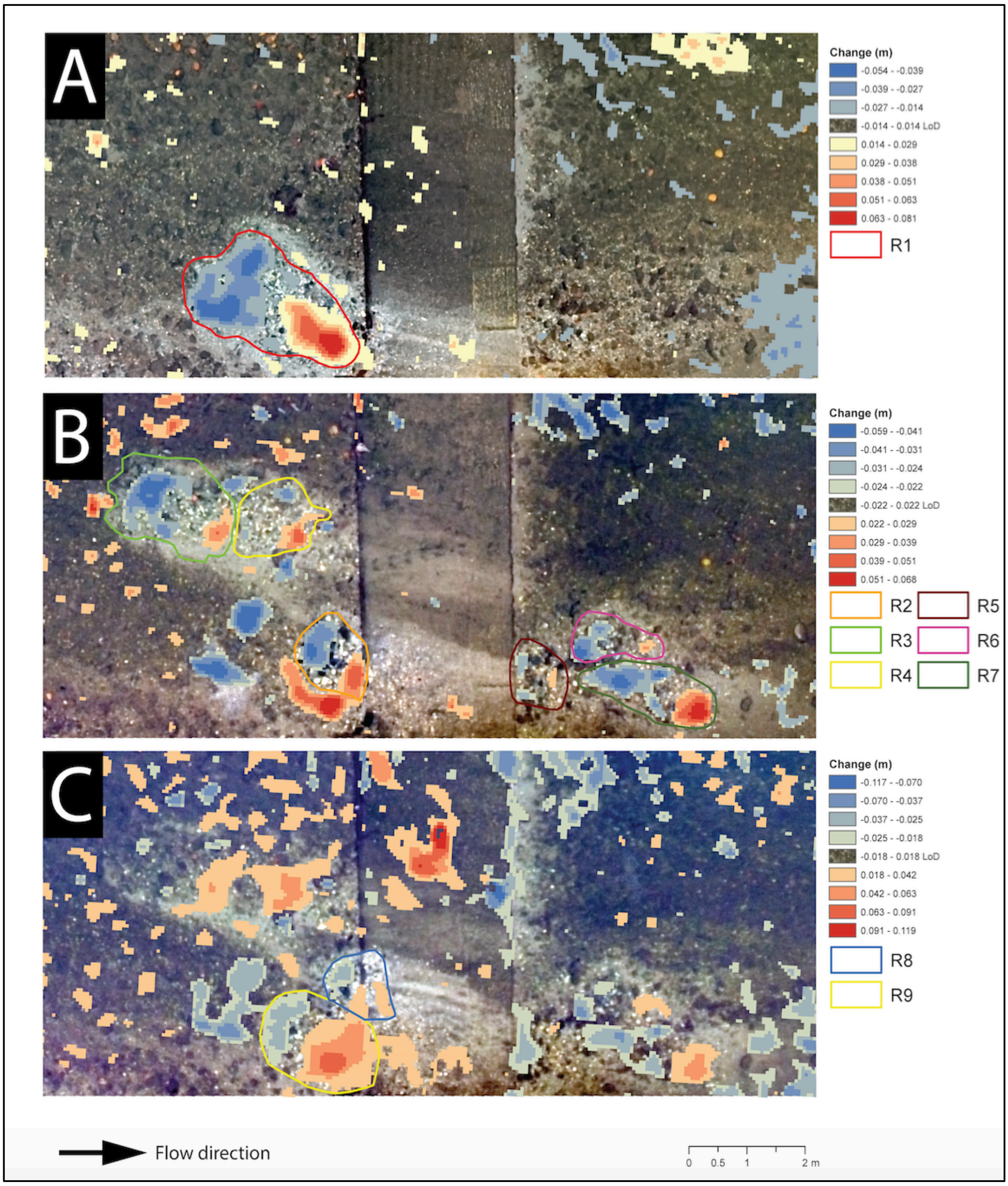

Figure 13: DEMs of Difference at the 68% confidence limit. Sub-figure A shows the changes between Nov. 11th and Nov. 19th; sub-figure B shows the changes between Nov. 11th and Dec. 2nd while sub-figure C shows the changes between Nov. 11th and Dec. 10th.

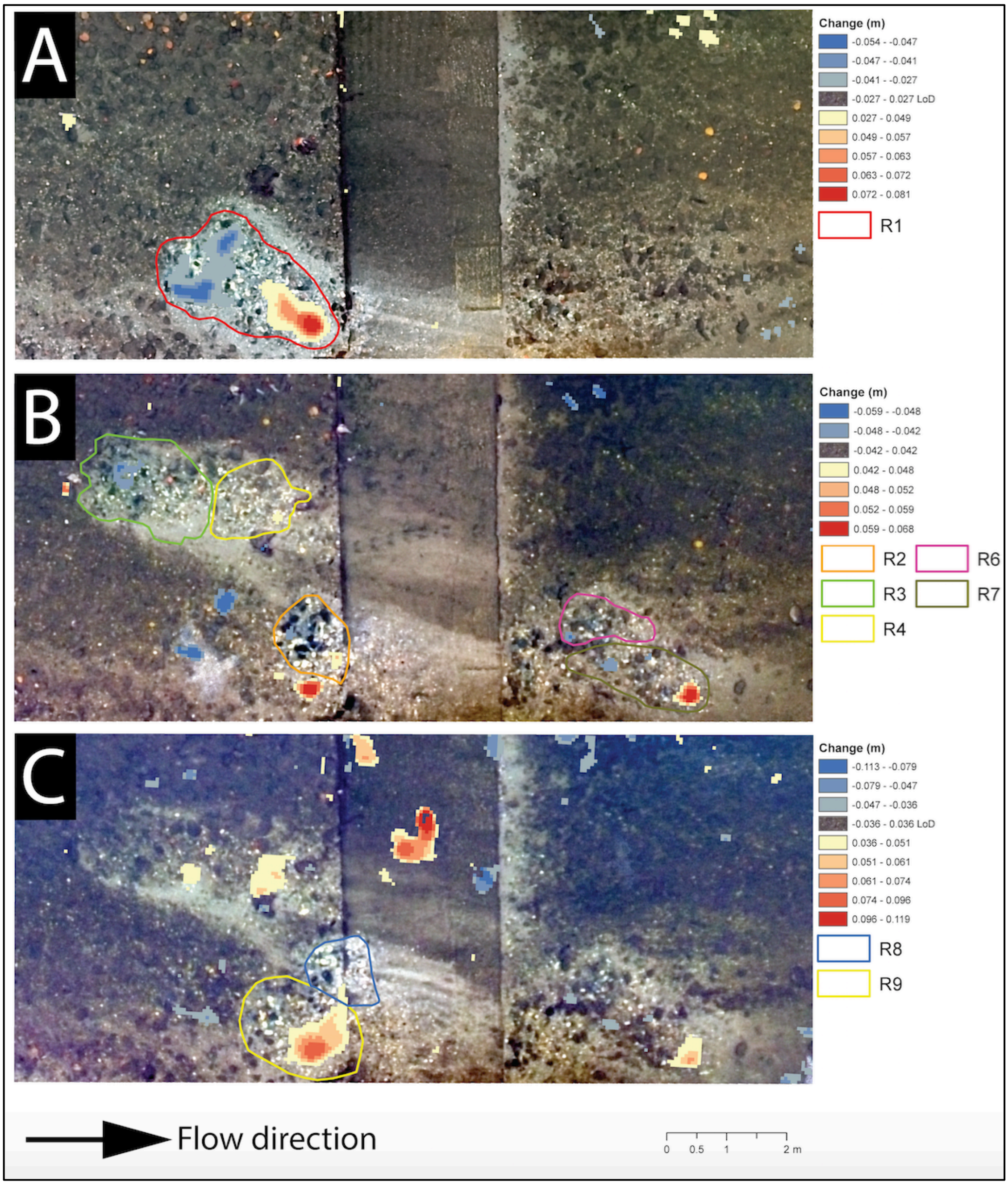

Figure 14: DEMs of Difference at the 95% confidence limit. Sub-figure A shows the changes between Nov. 11th and Nov. 19th; sub-figure B shows the changes between Nov. 11th and Dec. 2nd while sub-figure C shows the changes between Nov. 11th and Dec. 10th.

5.3 Redd characteristics

Spawning began around Nov. 19th and it ended approximately around Dec. 10th, which means that the season was relatively short (21 days). The site used to spawn was small compared to the full area studied (Figure 15). In fact, trout used approximately

~77.8 m^2 out of ~849.4 m^2 (~9.2%) with a redd area of ~14.1 m^2 (based on redds identified using the 68% confidence interval).

Figure 15: Spawning site (red rectangle) compared to the studied Breggia reach. On the left, out of image bounds, spawning habitat is limited by a deep pool generated by an artificial waterfall of ~4 m while on the right, out of image bounds, spawning is limited by a sandy and macrophytes-based pool. The orthomosaic presents the situation before spawning, on Nov. 11th.

Assuming that the 9 redds detected in the Breggia spawning site with the raw DoD and the 68% C.L. DoD are true redds, we measured the length of the tails and we estimated female lengths and the basal burial depths of eggs (Table 3).

Table 3: Estimated female length and basal burial depth from tail length for the Breggia Spawning site.

Date	Redd	Tail length (cm)	Estimated female length (cm)	Estimated egg burial depth (cm)
Nov. 19th	R1	166.9	48.9	16.7
Dec. 2nd	R2	68.3	23.2	6.3
Dec. 2nd	R3	72.2	24.3	6.9
Dec. 2nd	R4	74.2	24.9	7.3

Dec. 2nd	R5	47.4	17.1	2.1
Dec. 2nd	R6	76.9	25.63	7.7
Dec. 2nd	R7	92.3	29.8	9.8
Dec. 10th	R8	84.6	27.7	8.8
Dec. 10th	R9	149.7	44.7	15.5

Estimated female lengths varied from 17.1 cm to 48.9 cm with a mean size of 29.6 cm and a standard deviation of ±10.4 (Table 3). Curiously, four of the six female lengths estimated for Dec. 2nd are similar (σ_{length} = ±1.02), which might mean that it was only one instead of four female trout that produced R2, R3, R4 and R6. The estimated female length for R5 seems to be too small (17.1 cm) for a sexually mature trout.

Estimated basal burial depths varied from the minimum of 2.1 cm to the maximum of 16.7 cm with a mean depth of 9 cm and a standard deviation of ±4.6 (Table 3). The estimated basal burial depths may be analysed to understand if later spawners eroded previous redds.

Figure 16: Sub-figure A shows the DoD between Nov. 19th and Dec. 2nd with the respective redds while sub-figure B the DoD between Nov. 19th and Dec. 10th with the respective redds.

From Figure 16 it appears that R2 was partially created on the tail sediments of R1, however the female erosion does not reach the egg basal burial depth of R1 because the maximum pit depth of R2 is 5.2 cm. In addition to this, the pit was created only on one side of the R1 tail, reducing the probability of egg pocket destruction. By contrast, the R9 pit was created totally on the R1 tail, which might mean that eggs located in R1 were eroded and lost. However, as for R2, the maximum depth reached in the creation of the R9 pit (5.8 cm) did not reach the basal burial depth of R1 (16.5 cm). Consequently, the sediments might have naturally protected eggs pockets located near the basal depth of R1 even if the R9 pit was created where R1 eggs were laid. Clearly, one or more egg pockets might have been in upper layers and consequently they might have been destroyed by R9. Even with doubt over R5 and a certain probability of some R9 egg pockets being destroyed, we finally consider a total of 9 redds in this 10 m reach of the Breggia site.

6. Discussion

6.1 The use of UASs in surveying redds

The potential resolution of the images acquired is a strength of sUASs (Lejot et al., 2007; Niethammer et al., 2012) and, as implicit in [5], lower resolution imagery implies lower vertical precision but allows higher flights so covering larger areas more rapidly (Westoby et al., 2012). Thus, the operator has substantial opportunity to control data acquisition and quality (e.g. evaluate U_{crit}), depending on the specific research aim. This is why a critical element of the framework proposed here is the evaluation of the necessary theoretical vertical precision using [5] such that the UAS can be flown as high as possible so maximizing areal coverage, and consequent redd detection extent. Current developments of drone technology (e.g. GPS positioning) do not require manual-flight modes but allow for the use of pre-programmed flight paths, which can be designed to specifically meet the requirements of subsequent post-processing (Carbonneau et al., 2012) and data quality that is sought.

UASs represent three weaker points. First, weather conditions may limit the use of UASs, in particular strong winds and rain. Cold or hot temperatures can also limit the autonomy of batteries, reducing the performance of the drone. Second, battery autonomy is a key point in survey and planning, in fact the area covered by UASs is strictly dependent on the autonomy of batteries and on the number of batteries carried with in the survey. Third, the water should be clear enough (i) to be able to correct bathymetry and (ii) to be able to detect redds. In turbid rivers the use of UASs and SfM photogrammetry to characterized streambed topography is not appropriate, at least for bathymetric corrections based on Snell's law, which requires sufficient texture for point matching. Lastly, regulation restrictions refer to the legal principles regarding drone use and each country has normally its own. These rules may not only impact on whether or not UAS can be used but also how it has to be used. For instance, in Switzerland, line of sight has to be maintained during drone use, which restricts the spatial extent of any one flight path.

In our application, our study site was *c.* 70 m long and 60 m wide, and took no more than 30/35 minutes to be surveyed with 4 flight paths (including the time to set up, set down and change the batteries of the drone). This means that potentially, in a setting similar to that presented here, almost 1000 m in length can be mapped in 8 hours of work. If there is prior knowledge of where spawning is possible then this may allow longer total river reaches to be measured by focusing upon known spawning grounds. This may be aided by observations that salmonids that salmonids usually return to the same spawning grounds season after season (Dittman and Quinn, 1996).

6.2 Error assessment and management

The DEMs were initially affected by a negative datum shift. Here, our initial created DoDs were dominated by apparent erosion (Figure 7). This problem was reflected in the associated mean errors (Table 1) and error distributions (Figure 11A) between our reference DEM and the analysed DEMs for areas of no-known change between surveys. Datum shift removal improved DEM quality (Table 1, Figure 11B) but bathymetric correction was also needed to remove the mean error to negligible levels (Table 1, Figure 11C) and to reproduce redds that were apparent in orthorectified images (Figures 10 and 12). It is worth noting that in this study, a datum shift was found, rather than doming (James and Robson, 2014; Carbonneau and Dietrich, 2017), and this may reflect the survey design adopted here (multiple flying heights, inclusion of off-nadir imagery) which was designed to minimize doming effects (Robson et al., 1992; Wackrow and Chandler, 2011; James and Robson, 2014; Carbonneau and Dietrich, 2017). As mentioned earlier in this paper, the datum shift recorded here was attributable to the absence of GCPs on the right side of the channel, which led to poor transpositions of the point clouds to the absolute coordinate system. This was overcome by registering the analysed DEMs to our pre-spawning reference with the ICP algorithm.

Bathymetric correction was also crucial to reconcile the effects of flow variability (potentially also erosion and deposition which influences water depths locally) upon streambed bathymetry. This demonstrates the importance of the bathymetric corrections identified by Westaway et al. (2000, 2001) and the solution developed by Dietrich (2017) for SfM photogrammetry.

The precision, as expected, was not substantially impacted upon by either the datum shift or the bathymetric correction. The standard deviation of errors of ±10, ±13 and

±15 mm (Table 1) correspond to levels of detection of ±14, ±18 and ±22 mm with a 68% confidence level, and ±27, ±36 and ±42 mm at the 95% level. These latter values should be the same as (or slightly greater than; James et al., 2017b) the theoretically-predicted precision (U_{crit}) of ±24 mm (from [5]) given the survey design and UAS used, if all other influences on data error have been minimised. Only one LoD is really near U_{crit} (±27 mm); the other two LoD (±36 and ±42 mm) are higher (±12 and ±18 mm) compared with U_{crit}. This is common in photogrammetric studies as there is some degradation of survey precision from ideal or theoretical conditions (James et al., 2017b). However the results are encouraging, and suggest that [5] is a good means of identifying the survey design necessary for redd detection.

We found some evidence to suggest that an LoD threshold at 68% was appropriate (Lane et al., 2003) as redd changes are spatially coherent and one possible development of what we report here would be to integrate the Wheaton et al. (2010) treatment of coherence in DEMs of difference so as to reduce the probability of false negatives (small magnitude but spatially coherent changes that fall within the 95% detection limits). Given the spatial coherence of redd related changes, a lower detection threshold seems to be appropriate.

6.3 Morphological change versus visual detection

A key finding from this research is the advantage of quantifying redds and their dynamics in 3D using DoDs. Comparisons between Figures 12 and 13 show why interpretation of orthoimagery on its own is dangerous as it is biased by the redd age and consequent redd masking, something reported by others (e.g. Rieman and McIntyre, 1996; Gallagher and Gallagher, 2005). We suggest that this is a primary advantage of working with DEMs of difference rather than just orthoimagery.

Figures 9 and 13 identify more redds than were visible in the orthoimagery, and would likely have been identified in a walkover survey. This is of particular interest because reliable monitoring programs need unbiased redd counts (Gallagher and Gallagher, 2005). Our approach is less sensible to redd aging and masking by, for example, periphyton development. It also discrimination of superimposed redds, which is another source of error in classic redd counting (Dunham et al., 2001; Muhlfeld et al., 2006). The method is non-contact, avoiding redd disturbance.

6.4 Biological assessment

The Breggia spawning site does not only give us the possibility to demonstrate how new remote sensing technologies may help fish biology and water management but it also lends itself to a biological assessment. Spawning began around Nov. 19th (first detected redd) and it ended around Dec. 10th (last detected redds), with a total season length of 21 days. The spawning time was relatively short compared with the literature, which suggests for Switzerland a long spawning season, from October to January (Riedl and Peter, 2013). Previous research has shown that spawning season depends on both biotic and abiotic factors including genetic background (Quinn et al., 2000; Keller et al., 2011), river altitude (Riedl and Peter, 2013) and mean water temperature (Heggberget et al., 1988; Webb and McLay, 1996; Klemetsen et al., 2003). In the absence of data about mean water temperatures at the Breggia spawning site, we assume that spawning began when the conditions for reproduction were more suitable for brown trout. In this sense, and in addition to water temperatures, water velocities and water depths (see Armstrong et al., 2003) in the spawning site had to be ideal throughout these 21 days, or at least during the 9 spawning episodes.

The surface used to spawn by trout was small compared with the total inundated area investigated (see Figure 6). Here, the reason might be the limited availability of good spawning habitat (Armstrong et al., 2003), which confines spawning to such a small area. However, this also might mean a low productivity of the stretch. In this sense, Armstrong et al. (2003) argued that in case of a high density of spawners, some fish might be forced to spawn in poor habitat (e.g. outside the limits of the spawning area investigated), but the low density of spawning here suggests that this was not the case.

The data also suggested that redd superposition occurred throughout the season. Redd superposition is well documented in the scientific literature (Witzel and MacCrimmon, 1983; Sorensen et al., 1995) and it is typically explained by a limited spawning habitat availability (Ligon et al., 1995) or by spawning behaviour (Witzel and MacCrimmon, 1983; Essington et al., 1998). Either assumption could apply here. Following the behavioural point of view, Essington et al. (1998) argued that trout might choose a site previously used by another one just because it is more attractive, and not because habitat is limited. Grain dislocations by earlier spawners might induce later spawners to use the same grounds just because grains are less compacted and they are easier to move (Kondolf, 2000). Redd superimposition has a biological relevance for the success of spawning. The construction of a new redd on top of an old one normally means dispersion and loss of the older eggs (Hayes, 1987). Our results suggest however that later redd pits do not necesaarily reach the basal depth of the eggs pockets in the Breggia site, meaning that not all eggs have been washed-out. Egg pockets might be washed out if they were located in the upper sediments layers. This is also compounded by the possibility that flat, streambed-oriented stones in the sediment column under the redd sites have forced trout to lay their eggs at a lower depth (Crisp and Carling, 1989) compared with the predicted one. The ability to look at the vertical geometry of redds using the methods we present is a particular advantage.

We observed 4 redds with similar tail sizes (R2, R3, R4 and R6), which means similar female lengths and that they were constructed by the same female. However, a visual analysis of the Dec. 2nd orthomosaic suggests that R5, R6 and R7 were constructed before R2, R3 and R4. This makes sense because the color gradients of R5, R6 and R7 are less important compared with the other three. Under this assumption, we suppose that there are high probabilities that a single female created R2, R3 and R4 in the same spawning period. Considering that a female usually creates only one redd per spawning season (Crisp, 2000), R3 and R4 may be false redds without eggs, possibly because the trout did not find satisfactory conditions after a first cut session and decided to abandon the site (Crisp, 2000). According to Gallagher et al. (2007), fresh and real redd pits have an undisturbed sub-surface gravel-bed, which is normally composed of a dominant pebble matrix. R2 clearly shows this undisturbed gravel-bed while R3 and R4 show only a rough sediment matrix.

Some doubts emerged regarding R5 because of its size, smaller than the others, and the consequent estimated female length. In fact, the estimated female length of 17.11 cm seems to be too small for a mature trout in a low altitude river like the Breggia. In the Platte River (Michigan, US), Taube (1976) recorded sexual maturity from 17.7 cm, however the majority of females were sexually mature from 20.2 to 22.7 cm. Even if the comparison with the Breggia is difficult, the data recorded by Taube (1976) might validate our measurements for R5. There is also the possibility, nevertheless too complicated to demonstrate, that R5 is a false redd constructed by the R6 female.

From a biological point of view, doubts on the real extent of spawning in this site remain. These are compounded by the impossibility to know a priori (i.e. without look inside the redd, e.g. freeze-coring) if redds contain eggs or not.

7. Conclusions

This paper shows that salmonid redds may be detected through the combination of UASs and Structure-from-Motion photogrammetry, using morphological change instead of color gradients. Morphological changes are less sensitive to the evolution of the streambed in normal hydraulic conditions and this may be an advantage. Using the method, we show that it is also possible to quantify redd superposition, something that is particularly hard to identify visually, and also to understand the ecology of redd formation in more detail, such as the extent to which superposition of redds leads to destruction of the older redd. Crucial here is the derivation, correction and interpretation of DEMs of Difference, something that is increasingly straightforward given advances in our understanding of SfM photogrammetry, but which still requires careful study design. The main limit is use of the method under full or partial vegetation cover or in turbid water. In theory, the spatial scale of the survey method is defined simply by the time required to obtain imagery and necessary ground control. However, we emphasise that different countries and regions have different rules regarding drone use and these may limit the ease with which spatially extensive surveys may be undertaken.

Acknowledgements

This research did not receive any specific grant from funding agencies in the public, commercial, or not-for-profit sectors. The technical department of Vacallo and Mirco Ricci (the national Border Guard of Switzerland) gave permission to fly the drone on the Breggia river. Dr. Patrice Carbonneau and an anonymous reviewer are thanked for the detailed and critical but constructive comments and suggestions provided on earlier version of this article.

References

Armstrong, J.D., Kemp, P.S., Kennedy, G.J.A., Ladle, M. (2003). Habitat requirements of Atlantic salmon and brown trout in rivers and streams. Fisheries Research, 62, 143-170.

Bergeron, N., Carbonneau, P.E. (2012). Geosalar: Innovative Remote Sensing Methods for Spatially Continuous Mapping of Fluvial Habitat at Riverscape Scale. In Carbonneau and Piégay (ed.), Fluvial Remote Sensing for Science and Management, Oxford: Wiley-Blackwell, 193-213

Besl, P. J., McKay, N. D. (1992, April). Method for registration of 3-D shapes. In Sensor Fusion IV: Control Paradigms and Data Structures, 1611, 586-607

Bisson, P., Dunham, J., Reeves, G. (2009). Freshwater ecosystems and resilience of Pacific salmon: habitat management based on natural variability. Ecology and Society, 14(1), 45.

Bjornn, T. C., & Reiser, D. W. (1991). Habitat requirements of salmonids in streams. *American Fisheries Society Special Publication*, *19*(837), 138.

Borsuk, M.E., Reichert, P., Peter, A., Schager, E., Burkhardt-Holm, P. (2006). Assessing the decline Modelling, 192, 224-244.

Bradford, M.J., Irvine, J.R. (2000). Land use, fishing, climate change, and the decline of Thompson River, British Columbia, coho salmon. Canadian Journal of Fisheries and Aquatic Sciences, 57, 13-16.

Brasington, J., Rumsby, B. T., McVey, R. A. (2000). Monitoring and modelling morphological change in a braided gravel-bed river using high resolution GPS-based survey. Earth Surface Processes and Landforms, 25, 973-990.

Burner, C. J. (1951). Characteristics of spawning nests of Columbia River salmon. Fishery US Department of the Interior Bulletin of the Fish and Wildlife Service, 52, 97-110.

Butler, J.B., Lane, S.N., Chandler, J.H. (2001). Automated extraction of grain-size data from gravel surfaces using digital image processing. Journal of Hydraulic Research, 39, 519-529.

Carbonneau, P. E., Lane, S. N., & Bergeron, N. E. (2004). Catchment-scale mapping of surface grain size in gravel bed rivers using airborne digital imagery. Water Resources Research, 40, W07202

Carbonneau, P. E., Bergeron, N., Lane, S. N. (2005). Automated grain size measurements from airborne remote sensing for long profile measurements of fluvial grain sizes. Water Resources Research, 41, W11426

Carbonneau, P.E., Piégay, H., Lejot, J., Dunford, R., Michel, K. (2012). Hyperspatial Imagery in Riverine Environments. In Carbonneau and Piégay (ed.), Fluvial

Remote Sensing for Science and Management Oxford: Wiley-Blackwell, 163-191

Carbonneau, P.E. and Dietrich, J.T. (2017). Cost-effective non-metric photogrammetry from consumer-grade sUAS: implications for direct georeferencing of structure from motion photogrammetry. Earth Surface Processes and Landforms, 42, 473-486.

Crisp, D.T. and Carling, P.A. (1989). Observation on siting, dimensions and structure of salmonid redds. Journal of Fish Biology, 34, 119-134.

Crisp, D.T. (2000). Trout and salmon: ecology, conservation and rehabilitation. Hoboken : Wiley-Blackwell.

DeVries, P. (1997). Riverine salmonid egg burial depths: review of published data and implications for scour studies. Canadian Journal of Fisheries and Aquatic Sciences, 54, 1685-1698.

Dietrich, J.T. (2016). Riverscape mapping with helicopter-based Structure-from-Motion photogrammetry. Geomorphology, 252, 144-157.

Dietrich, J.T. (2017). Bathymetric Structure-from-Motion: extracting shallow stream bathymetry from multi-view stereo photogrammetry. Earth Surface Processes and Landforms, 42, 355-364.

Dittman, A., & Quinn, T. (1996). Homing in Pacific salmon: mechanisms and ecological basis. *Journal of Experimental Biology*, *199*(1), 83-91.

Elliot, J.M. (1994). Quantitative ecology and the brown trout. New York : Oxford University Press Inc..

Essington, T. E., Sorensen, P. W., Paron, D. G. (1998). High rate of redd superimposition by brook trout (Salvelinus fontinalis) and brown trout (Salmo trutta) in a Minnesota stream cannot be explained by habitat availability alone. Canadian Journal of Fisheries and Aquatic Sciences, 55, 2310-2316.

Fisher, P.F. and Tate, N.J. (2006). Causes and consequences of error in digital elevation models. Progress in Physical Geography, 30, 467-489.

Fonstad, M.A., Dietrich, J.T., Courville, B.C., Jensen, J.L., Carbonneau, P.E. (2013). Topographic structure from motion: a new development in photogrammetric measurement. Earth Surface Processes and Landforms, 38, 421-430.

Fryer, J.G. (1983). A simple system for photogrammetric mapping in shallow water. The Photogrammetric Record, 11, 203-208.

Fryer, J.G., Kniest, H.T. (1985). Errors In Depth Determination Caused By Waves In Through-Water Photogrammetry. The Photogrammetric Record, 11, 745-753.

Fuller, I.C., Large, A.R., Charlton, M.E., Heritage, G.L., Milan, D.J. (2003). Reach-scale sediment transfers: An evaluation of two morphological budgeting approaches. Earth Surface Processes and Landforms, 28, 889-903.

Gallagher, S. P., & Gallagher, C. M. (2005). Discrimination of Chinook salmon, coho salmon, and steelhead redds and evaluation of the use of redd data for estimating escapement in several unregulated streams in northern California. *North American Journal of Fisheries Management*, *25*(1), 284-300.

Gallagher S.P., Hahn, P.K.J., Johnson, D.H (2007). Redd counts. In D.H. Johnson, B.M. Shrier, J.S., O'Neal, J.A. Knutzen, X. Augerot, T.A. O'Neil and T.N. Pearsons (eds), Salmonid Field Protocols Handbook, Bethesda: American Fisheries Society, pp. 163-191

Grost, R.T., Hubert, W.A., Wesche, T.A. (1991). Description of brown trout redds in a mountain stream. Transactions of the American Fisheries Society, 120, 582-588.

Groves, P.A., Alcorn, B., Wiest, M. M., Maselko, J. M., Connor, W. P. (2016). Testing unmanned aircraft systems for salmon spawning surveys. FACETS, 1, 187-204.

Healey, M.C. (1991). Life history of chinook salmon (Oncorhynchus tshawytscha). In C. Groot and L. Margolis (eds.), Pacific salmon life histories, Vancouver: UBC Press, 311-394

Harvey, A.H., Gallagher, J.S., Sengers, J. L. (1998). Revised formulation for the refractive index of water and steam as a function of wavelength, temperature and density. Journal of Physical and Chemical Reference Data, 27, 761-774.

Hayes, J.W. (1987). Competition for spawning space between brown (Salmo trutta) and rainbow trout (S. gairdneri) in a lake inlet tributary, New Zealand. Canadian Journal of Fisheries and Aquatic Sciences, 44(1), 40-47. doi: 10.1139/f87-005

Heggberget, T.G., Haukebø, T., Mork, J., Ståhl, G. (1988). Temporal and spatial segregation of spawning in sympatric populations of Atlantic salmon, Salmo salar L., and brown trout, Salmo trutta L. Journal of Fish Biology, 33, 347-356.

Hendry, K., Cragg-Hine, D., O'Grady, M., Sambrook, H., Stephen, A. (2003). Management of habitat for rehabilitation and enhancement of salmonid stocks. Fisheries Research, 62, 171-192.

Howell, P. J., & Sankovich, P. M. (2012). An evaluation of redd counts as a measure of bull trout population size and trend. *North American Journal of Fisheries Management*, *32*(1), 1-13.

James, M.R. and Robson, S. (2014). Mitigating systematic error in topographic models derived from UAV and ground-based image networks. Earth Surface Processes and Landforms, 39, 1413-1420.

James, M.R., Robson, S., d'Oleire-Oltmanns, S., Niethammer, U. (2017a). Optimising UAV topographic surveys processed with structure-from-motion: Ground control quality, quantity and bundle adjustment. Geomorphology, 280, 51-66.

James, M.R., Robson, S., Smith, M.W. (2017b). 3-D uncertainty-based topographic change detection with structure-from-motion photogrammetry: precision maps for ground control and directly georeferenced surveys. Earth Surf. Process. Landforms, 42, 1769– 1788

Keller, I., Taverna, A., Seehausen, O. (2011). Evidence of neutral and adaptive genetic divergence between European trout populations sampled along altitudinal gradients. Molecular Ecology, 20, 1888-1904.

Klemetsen, A., Amundsen, P.A., Dempson, J.B., Jonsson, B., Jonsson, N., O'connell, M.F., Mortensen, E. (2003). Atlantic salmon Salmo salar L., brown trout Salmo trutta L. and Arctic charr Salvelinus alpinus (L.): a review of aspects of their life histories. Ecology of Freshwater Fish, 12, 1-59.

Kondolf, G.M. (2000). Assessing salmonid spawning gravel quality. Transactions of the American Fisheries Society, 129, 262-281.

Kondolf, G.M., Williams, J.G., Horner, T.C., Milan, D.A.V.I. D. (2008). Assessing physical quality of spawning habitat. In American Fisheries Society Symposium, 65, 000-000

Lane, S.N., Richards, K.S., & Chandler, J.H. (1994). Developments in monitoring and modelling small-scale river bed topography. Earth Surface Processes and Landforms, 19, 349-368.

Lane, S.N., Westaway, M., Hicks, D.M. (2003). Estimation of erosion and deposition volumes in a large, gravel-bed, braided river using synoptic remote sensing. Earth Surface Processes and Landforms, 28, 249-271.

Lane, S. N., Reid, S. C., Westaway, R. M., & Hicks, D. M. (2004). Remotely sensed topographic data for river channel research: the identification, explanation and management of error. In Kelly R.E.J., N.A. Drake and S.L. Barr, Spatial

Modelling of the Terrestrial Environment West Sussex: John Wiley & Sons, Ltd., 113-136

Lane, S. N., Widdison, P. E., Thomas, R. E., Ashworth, P. J., Best, J. L., Lunt, I. A., Sambrook Smith, G. H. & Simpson, C. J. 2010). Quantification of braided river channel change using archival digital image analysis. Earth Surface Processes and Landforms, 35, 971-985.

Lejot, J., Delacourt, C., Piégay, H., Fournier, T., Trémélo, M.-L., Allemand, P. (2007). Very high spatial resolution imagery for channel bathymetry and topography from unmanned mapping controlled platform. Earth Surface Processes and Landforms, 32, 1705-1725.

Ligon, F.K. (1995). Downstream Ecological Effects of Dams. BioScience, 45, 183-192.

Marteau, B., Vericat, D., Gibbins, C., Batalla, R.J., Green, D.R. (2017). Application of Structure-from-Motion photogrammetry to river restoration. Earth Surface Processes and Landforms, 42, 503-515.

Maxell, B. A. (1999). A power analysis on the monitoring of bull trout stocks using redd counts. *North American Journal of Fisheries Management*, *19*(3), 860-866.

Micheletti, N., Chandler, J.H., Lane, S.N. (2015a). Structure from motion (SFM) phogrammetry. In Cook, S.J., Clarke, L.E., Nield, J.M. (eds.), Geomorphological Techniques (Online Edition). British Society for Geomorphology: London.

Micheletti, N., Chandler, J.H., Lane, S.N. (2015b). Investigating the geomorphological potential of freely available and accessible structure-from-motion photogrammetry using a smartphone. Earth Surface Processes and Landforms, 40, 473-486.

Milan, D.J., Heritage, G. L., Large, A. R., Fuller, I. C. (2011). Filtering spatial error from DEMs: Implications for morphological change estimation. Geomorphology, 125, 160-171.

Muhlfeld, C. C., Taper, M. L., Staples, D. F., & Shepard, B. B. (2006). Observer error structure in bull trout redd counts in Montana streams: implications for inference on true redd numbers. *Transactions of the American Fisheries Society*, *135*(3), 643-654.

Murdoch, A. R., Pearsons, T. N., & Maitland, T. W. (2010). Estimating the spawning escapement of hatchery-and natural-origin spring Chinook Salmon using redd and carcass data. *North American Journal of Fisheries Management*, *30*(2), 361-375.

Neilson, J. D., & Banford, C. E. (1983). Chinook salmon (Oncorhynchus tshawytscha) spawner characteristics in relation to redd physical features. *Canadian Journal of Zoology*, *61*(7), 1524-1531.

Niethammer, U., James, M.R., Rothmund, S., Travelletti, J., Joswig, M. (2012). UAV-based remote sensing of the Super-Sauze landslide: Evaluation and results. Engineering Geology, 128, 2-11.

Ottaway, E.M., Carling, P.A., Clarke, A., & Reader, N.A. (1981). Observations on the structure of brown trout, Salmo trutta Linnaeus, redds. Journal of Fish Biology, 19, 593-607.

Pix4D (2017a). Pix4Dcapture. Available at https://pix4d.com/product/pix4dcapture (consulted the 21st May 2017).

Pix4D (2017b). Pix4Dmapper pro. Available at https://pix4d.com/product/pix4dmapper-pro/ (consulted the 21st May 2017).

Quinn, T.P., Unwin, M.J., & Kinnison, M.T. (2000). Evolution of temporal isolation in the wild: genetic divergence in timing of migration and breeding by introduced chinook salmon populations. Evolution, 54, 1372-1385.

Quinn, T.P. (2005). The behaviour and ecology of Pacific Salmon and Trout. Seattle: University of Washington Press.

Reiser, D.W., and Wesche, T A. (1977). Determination of physical and hydraulic preferences of brown and brook trout in the selection of spawning locations. Completion report for project C-7002. Water Research and Technology. Water Resources Research Institute, University of Wyoming, Laramie, W Y

Riedl, C. and Peter, A. (2013). Timing of brown trout spawning in Alpine rivers with special consideration of egg burial depth. Ecology of Freshwater Fish, 22, 384-397.

Rieman, B. E., & McIntyre, J. D. (1996). Spatial and temporal variability in bull trout redd counts. North American Journal of Fisheries Management, 16, 132-141.

Robson, S. (1992). Film deformation in non-metric cameras under weak geometric conditions-an uncorrected disaster?. International Archives of Photogrammetry and Remote Sensing, 29, 561-567

Simenstad, C.A., Cordell, J.R. (2000). Ecological assessment criteria for restoring anadromous salmonid habitat in Pacific Northwest estuaries. Ecological Engineering, 15, 283-302.

Sorensen, P.W., Essington, T., Weigel, D.E., Cardwell, J.R. (1995). Reproductive interactions between sympatric brook and brown trout in a small Minnesota stream. Canadian Journal of Fisheries and Aquatic Sciences, 52, 1958-1965.

Tamminga, A., Hugenholtz, C., Eaton, B., Lapointe, M. (2015). Hyperspatial Remote Sensing of Channel Reach Morphology and Hydraulic Fish Habitat Using an Unmanned Aerial Vehicle (UAV): A First Assessment in the Context of River Research and Management. River Research and Applications, 31, 379-391.

Taube, C.M. (1976). Sexual maturity and fecundity in brown trout of the Platte River, Michigan. Transactions of the American Fisheries Society, 105, 529-533.

Wackrow, R., Chandler, J. H. (2011). Minimising systematic error surfaces in digital elevation models using oblique convergent imagery. The Photogrammetric Record, 26, 16-31.

Webb, J.H., McLay, H.A. (1996). Variation in the time of spawning of Atlantic salmon (Salmo salar) and its relationship to temperature in the Aberdeenshire Dee, Scotland. Canadian Journal of Fisheries and Aquatic Sciences, 53, 2739-2744.

Westaway, R.M., Lane, S.N., Hicks, D.M. (2000). The development of an automated correction procedure for digital photogrammetry for the study of wide, shallow, gravel-bed rivers. Earth Surface Processes and Landforms, 25, 209-226.

Westaway, R.M., Lane, S.N., Hicks, D.M. (2001). Remote sensing of clear-water, shallow, gravel-bed rivers using digital photogrammetry. Photogrammetric Engineering and Remote Sensing, 67, 1271-1282.

Westoby, M.J., Brasington, J., Glasser, N.F., Hambrey, M.J., Reynolds, J.M. (2012). 'Structure- from-Motion' photogrammetry: A low-cost, effective tool for geoscience applications. Geomorphology, 179, 300-314.

Wheaton, J.M., Brasington, J., Darby, S.E., Sear, D.A. (2010). Accounting for uncertainty in DEMs from repeat topographic surveys: improved sediment budgets. Earth Surface Processes and Landforms, 35, 136-156.

Witzel, L. D. and MacCrimmon, H. R. (1983). Embryo survival and alevin emergence of brook charr, Salvelinus fontinalis and brown trout, Salmo trutta, relative to redd gravel composition. Canadian Journal of Zoology, 61, 1783-1792.

Woodget, A.S., Carbonneau, P.E., Visser, F., Maddock, I.P. (2015). Quantifying submerged fluvial topography using hyperspatial resolution UAS imagery and structure from motion photogrammetry. Earth Surface Processes and Landforms, 40, 47-64.

Zimmerli, S., Bernet, D., Burkhardt-Holm, P., Schmidt-Posthaus, H., Vonlanthen, P., Wahli, T., Segner, H. (2007). Assessment of fish health status in four Swiss rivers showing a decline of brown trout catches. Aquatic Sciences, 69, 11-25.